Coronagraphy robust to segmented aberrations: low-wind effect mitigation on Subaru/SCExAO

Lucie Leboulleux, Olivier Guyon, Julien Lozi, Miles Lucas, Sébastien Vievard, Vincent Deo, Kyohoon Ahn, Alexis Carlotti, Alain Delboulbé, Mamadou N'Diaye, et al.

Coronagraphy robust to segmented aberrations: low-wind effect mitigation on Subaru/SCExAO

Lucie Leboulleux[a], Olivier Guyon[b,c,d,e], Julien Lozi[b], Miles Lucas[f], Sébastien Vievard[b,e], Vincent Deo[b], Kyohoon Ahn[b,g], Alexis Carlotti[a], Alain Delboulbé[a], Mamadou N'Diaye[h], Marie-Hélène Sztefek[b], and Philippe Delorme[b]

[a]Univ. Grenoble Alpes, CNRS, IPAG, 38000 Grenoble, France
[b]Subaru Telescope, National Astronomical Observatory of Japan, 650 N. Aohoku Pl., Hilo, HI 96720, USA
[c]College of Optical Sciences, University of Arizona, Tucson, AZ 87521, USA
[d]Steward Observatory, University of Arizona, Tucson, AZ 87521, USA
[e]Astrobiology Center, 2 Chome-21-1, Osawa, Mitaka, Tokyo, 181-8588, Japan
[f]Institute for Astronomy, University of Hawai'i, 640 N. Aohoku Pl., Hilo, HI 96720, USA
[g]Korea Astronomy and Space Science Institutde, 776 Daedeok-daero, Yuseong-gu, Daejeon 34055, Republic of Korea
[h]Université Côte d'Azur, Observatoire de la Côte d'Azur, CNRS, Laboratoire Lagrange, France

ABSTRACT

Low-wind effect is a strong limitation to direct imaging of exoplanets from ground-based telescopes, such as the Subaru telescope, the Very Large Telescope and probably the future extremely large telescopes. To mitigate it, we propose to design coronagraphs passively robust to low-wind effect. The Redundant Apodized Pupils (RAPs) are built so each pupil petal independently contributes to the contrast and therefore petal-level errors do not impact the final coronagraphic image, up to the loss of coherence in the star image. In this paper, we present the first experimental validation of the RAP concept, which is now applied on the Subaru/SCExAO instrument. We have designed three RAPs: two for the infrared channel (CHARIS) and one for the visible instrument (VAMPIRES). After these designs having been set up on the instrument in September 2023, we conducted internal source tests and obtained a contrast robustness up to a few radians. After this first experimental application, the RAP technology will be adapted, at higher contrasts (10^{-8}-10^{-9}), to segment-level errors, one of the main limitations for space segmented telescopes like the Habitable Worlds Observatory.

Keywords: Exoplanets, high-contrast imaging, instrumentation, robustness, low-wind effect, coronagraphy

1. INTRODUCTION

High-contrast imaging of exoplanets and disks requires a control of aberrations. Between others, the low-wind effect (LWE) is already a limitation on ground-based instruments when installed on high-emissivity spider telescopes: for instance, it was first measured and studied on the Spectro-Polarimetic High contrast imager for Exoplanets REsearch (SPHERE)[1] at the Very Large Telescope (VLT) by.[2–7] This phenomenon happens when the wind speed at the level of the telescope aperture is lower than a few m/s. Because of differential thermal cooling along the spiders, the phase is fragmented into piston, tip, and tilt at the scale of the petals delimited by the spiders.[8,9] These optical path differences, up to hundreds of nanometers cannot be corrected by traditional adaptive optics (AO) systems since they are based on wavefront sensors that only measure phase gradients and therefore remain insensitive to sharp discontinuities between wide pistons.[10] On science images, these differential pistons, tips, and tilts create secondary lobes around the location of the first Airy ring, distorting the PSF and degrading the Strehl ratio (see Figure 1). On coronagraphic images, this directly impacts the contrast, in addition

Further author information: (Send correspondence to L.L.)
E-mail: lucie.leboulleux@univ-grenoble-alpes.fr

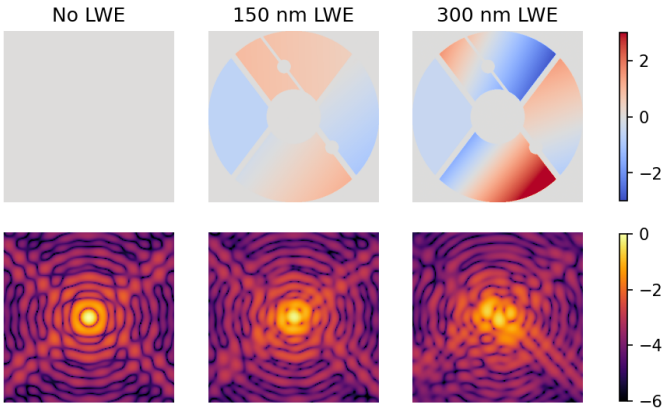

Figure 1. Simulation of low-wind effect on Subaru/SCExAO: (top) phase maps in radians with 0 to 300 nm RMS (at a 1.6 μm wavelength) of differential pistons, tips, and tilts, (bottom) associated PSFs in logarithmic scales with a field of view of $\pm 10\lambda/D$.

with these secondary lobes also acting like off-axis sources and generating starlight leakage along the focal-plane mask. In addition with VLT/SPHERE, this phenomenon has also been detected on other telescopes such as the Subaru Telescope/Subaru Coronagraphic Extreme Adaptive Optics instrument (SCExAO)[11–13] and, because of their wider spiders (respectively 51 cm and 225 mm wide spider), the future Extremely Large Telescope (ELT) and Thirty Meter Telescope (TMT) will probably also be sensitive to LWE.[8]

Because of its high degradation of the contrast on coronagraphic images and its impact on several telescopes, LWE is a strong limitation to overcome, and several mitigation strategies are under study. First, a thermal coating has been applied on the VLT spiders, leading to a drastic decrease in the aberration amplitude. In addition, focal plane wavefront sensors are more sensitive than pupil plane wavefront sensors to pupil and phase discontinuities.[11,13,14] A last mitigation strategy consists in a modification of the pupil apodization (amplitude or phase) to optimize the apodization at the scale of the petal and multiply it over the pupil to make it robust to differential piston, tip, and tilt errors between the pupil petals.[15,16] This concept is called the Redundant Apodized Pupil (RAP) and is the purpose of this paper.

The SCExAO instrument is a competitive science instrument equipped with extreme adaptive optics and also an experimental platform for instrumental research and development. It is set up at the Subaru telescope, a 8.2m large telescope built on the Mauna Kea, in Hawaii. With its sensitivity to LWE, its ability to mimic it with a deformable mirror (DM),[11–13] and its flexibility for experiments, SCExAO is an optimal platform to apply and test the RAP concept. The objective of the study presented here is then to propose and test coronagraphs robust to LWE on SCExAO, in both the near-infrared path with the Coronagraphic High Angular Resolution Imaging Spectrograph (CHARIS) and in the optical path with the Visible Aperture Masking Polarimetric Imager for Resolved Exoplanetary Structures (VAMPIRES), in internal source.

In section 2, we describe three RAPs that have been optimized for the Subaru/SCExAO, both in the optical path (VAMPIRES) and in the near-infrared path (CHARIS). In section 3, we describe the experimental set up on SCExAO and the data processing methodology. In section 4, the RAPs are applied and tested on both CHARIS and VAMPIRES with the internal sources and we introduce the first results. In section 5, we discuss this study and the advantages and drawbacks of RAP for further observations at Subaru/SCExAO and further technological developments on upcoming instruments.

2. REDUNDANT APODIZED PUPIL DESIGN

2.1 Constraints and design of RAPs for CHARIS

CHARIS is the Integral Field Spectrograph (IFS) at the Subaru telescope and is combined with the SCExAO coronagraphic instrument.[17–22] It covers infrared wavelengths from 0.95 to 2.4 μm, which imposes the main

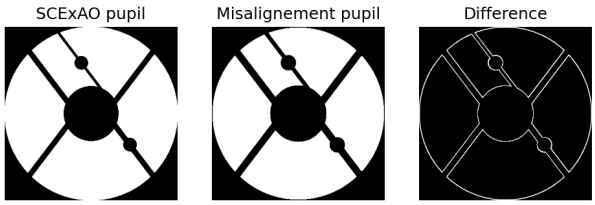

Figure 2. From left to right: Real SCExAO pupil, pupil chosen for the optimization, and difference between the two. The pupil transmissions are binary, 0 meaning no transmission and 1 full transmission.

constraints for the RAP design: the angular spatial resolution is 24 mas at 0.95 μm, and goes up to 60 mas at 2.4 μm. RAPs cannot access Inner Working Angles (IWA) below the petal diffraction limit (here below $\sim 2.5\lambda/D$) and hardly access low angular separations (lower than $6\lambda/D$) while preserving their throughputs. In our case, we decide to focus on different science target areas:

• a full donut-like dark zone, obtained with one single RAP (CHAR1), down to an average contrast of a few 10^{-6} from 7 to $33\lambda/D$, which enables to access targets from 420 to 800 mas while covering the entire CHARIS spectral bandwidth,

• a "prohibition" sign dark zone, obtained with so-called CHAR2, and down to an average contrast of a few 10^{-6} from 5 to $25\lambda/D$, which enables to access targets from 300 to 600 mas while covering the entire CHARIS spectral bandwidth. This prohibition sign shape has been chosen after originally designing two RAPs with complementary dark zones in bow tie shapes: they had very different throughputs, showing that one direction only in the dark zone is hard to dig in intensity and decreasas the apodizer throughput. This prohibition sign dark zone is a compromise between a large dark zone and avoiding that one single problematic direction. In addition, since this direction is of no interest, petals North and West are optimized together, and petals South and East too: island effects between South and East (resp. North and West) petals create a startlight leakage in the direction of no interest, ie., outside the dark region.

The pupil used for the optimization is chosen slightly smaller and with wider spiders and central obstruction than the real SCExAO pupil to allow for small misalignments ($\pm 0.5\%$ in all directions) when being installed. Figure 2 shows the real SCExAO pupil, the one chosen for the optimization, and the difference between the two.

With RAPs,[15,16] the mitigation of petal-level errors relies on the fact that each petal generates a low-order contribution to the full apodized pupil PSF with its own coronagraphic dark zone. These petal-level dark zones prevent the intensity from increasing even in presence of petal-level aberrations. Figure 3 illustrates the contribution of each apodized petal and their recombination (so-called RAP) on the PSF in monochromatic light, in the CHAR1 case, meaning for a 10^{-6} dark zone from 7 to $33\lambda/D$. As mentioned in Leboulleux *et al.* 2022,[16] one can notice that a complete RAP contrast of $\sim 10^{-6}$ requires each petal contrast to go down to only $10^{-4.5}$.

Figure 4 (left and center) shows all three RAPs assembled, optimized upon the specifications mentioned above. Figure 5 (top and center) shows the coronagraphic PSFs both in monochromatic light (0.95, 1.7, and 2.4 μm) and in broadband light ($0.95 - 2.4$ μm). In this latest image, the broadband PSF corresponds to an RGB combination, made of 41 coronagraphic PSFs with wavelengths equally spread between 0.95 and 2.4 μm, their intensities being allocated across the three RGB channels proportionally to their wavelength. Two planets down to contrasts of 5×10^{-5} and 10^{-5} are visible at respectively 450 mas and 600 mas. In addition, the final RAP specifications are indicated in table 1.

In narrower bands, CHAR1 enables to access from 234 to 976 mas in J band (1.176 to 1.328 μm), from 314 to 1237 mas in H band (1.490 to 1.783 μm), and from 418 to 1676 mas in K band (2.019 to 2.375 μm). CHAR2 can access from 167 to 740 mas in J band, from 224 to 937 mas in H band, and from 299 to 1270 mas in K band.

2.2 Constraints and design of a RAP for VAMPIRES

VAMPIRES is a visible-light instrument on the SCExAO system.[24–27] It can observe from 600 to 800 nm with five 50 nm bandpass filters centered at 625, 675, 725, 750, and 775 nm. At 600 nm (resp. 800 nm), the diffraction-limited FWHM is 15.6 mas per λ/D (resp. 20.8 mas per λ/D).

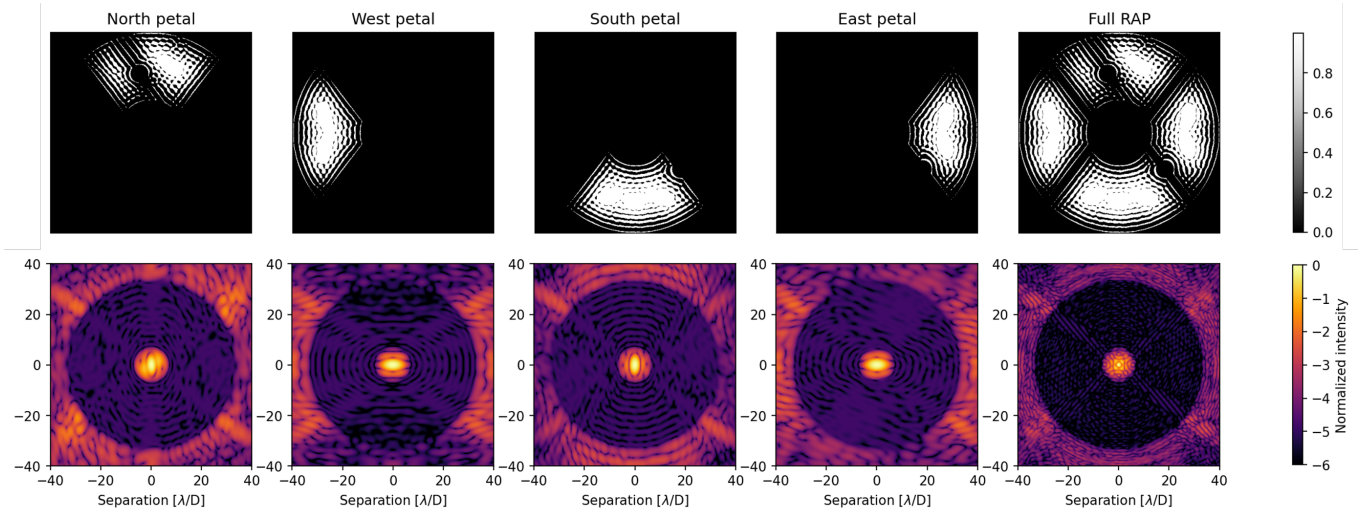

Figure 3. RAP combination in the CHAR1 case: (top) apodized petals and combined RAP, (bottom) associated PSFs in logarithmic scale. The apodized petals' and RAP transmissions are binary: 0 stands for no transmission and 1 for full transmission.

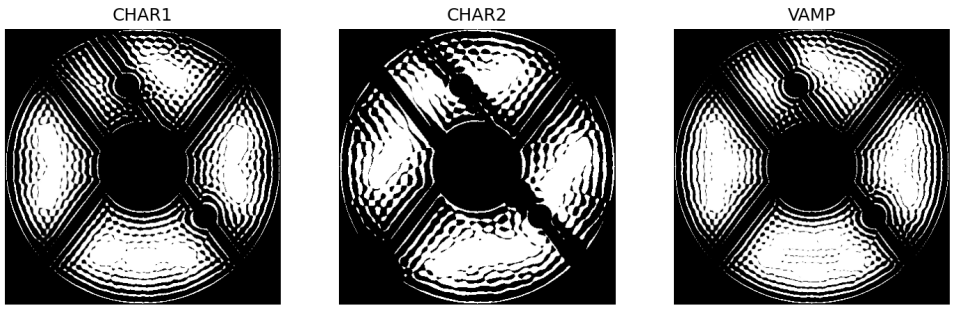

Figure 4. RAPs as amplitude apodizers aiming for the specifications indicated in Table 1. The pupil transmissions go from 0 (no transmission) to 1 (full transmission).

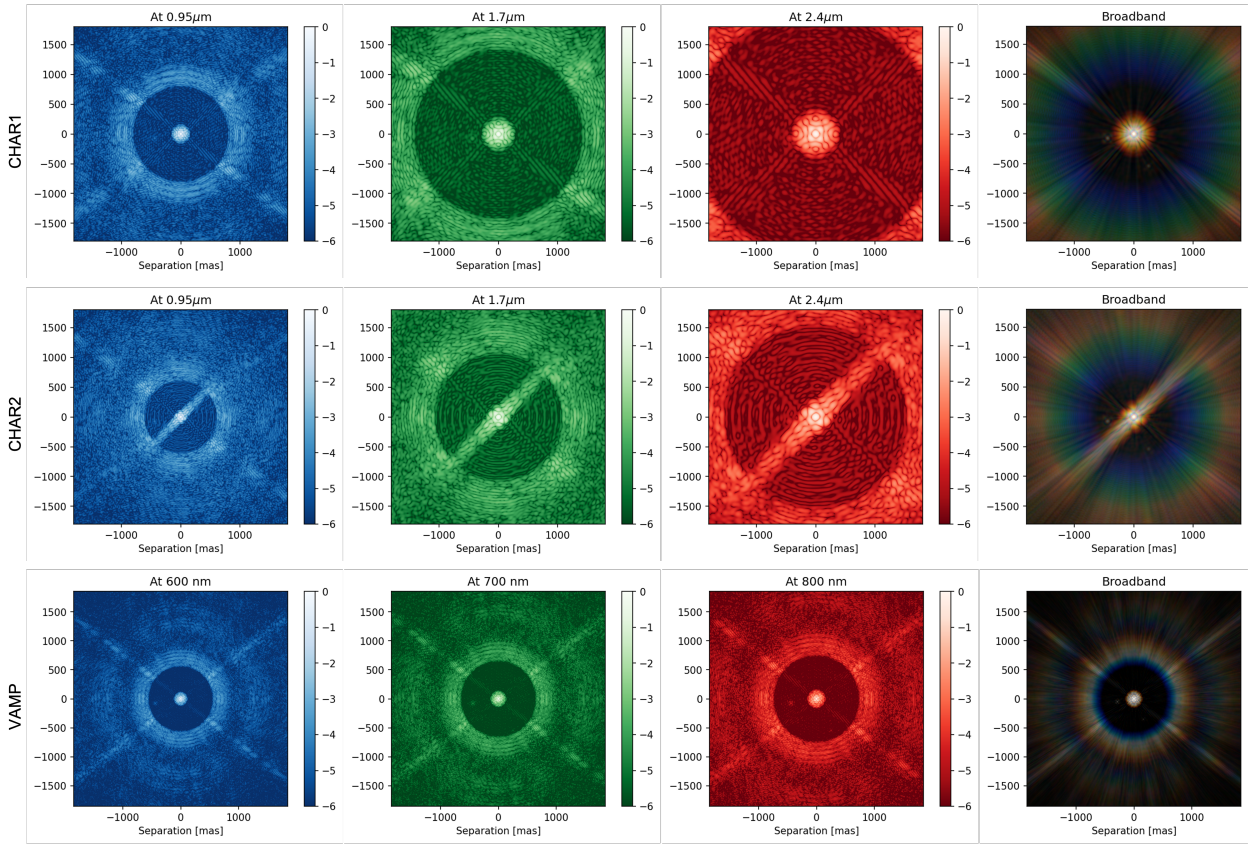

Figure 5. Coronagraphic PSFs with the three RAPs (from top to bottom: CHAR1, CHAR2, and VAMP) in monochromatic light (three first columns) and in broadband light (right column). The RAP designs are optimized to provide dark zones according to Table 1. Two planets down to contrasts of 5×10^{-5} and 10^{-5} are visible in the dark zones at respectively 450 mas and 600 mas. The broadband images correspond to an RGB combination, made of 41 coronagraphic PSFs with wavelengths equally spread between 0.95 and 2.4 μm for CHAR1 and CHAR2, and between 600 and 800 nm for VAMP, their intensities being allocated across the three RGB channels proportionally to their wavelength. All images are in logarithmic scales.

RAP	Contrast	IWA (λ/D)	OWA (λ/D)	Covered separations (mas)	Throughput
CHAR1	2.8×10^{-6}	7	33	420-800	22%
CHAR2	5.2×10^{-6}	5	25	300-600	25%
VAMP	8.9×10^{-7}	8	35	167-546	25%

Table 1. Specifications for the three RAP cases, CHAR1 and CHAR2 being designed for CHARIS, and VAMP being developed for VAMPIRES. CHAR2 accesses a prohibition sign shaped dark region (see Figure 5). The contrasts correspond to the average contrasts in the dark regions, and the covered separations correspond to the broadband light dark region (0.95 to 2.4 μm for CHARIS, 600 to 800 nm for VAMPIRES). The throughputs are computed according to Ruane *et al.* 2018.[23]

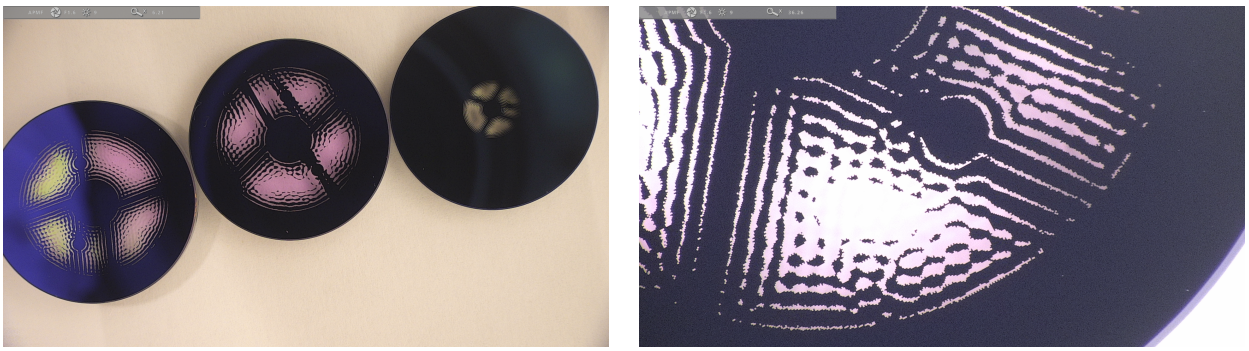

Figure 6. Apodizers provided by Optimask under a microscope: (left) from left to right: CHAR1, CHAR2, and VAMP, (right) zoom in on CHAR1, where each pixel can be identified. For CHAR1 and CHAR2 (resp. VAMP), each pixel measures 35μm (resp. 10μm).

Using again the misalignment pupil of Figure 2, another RAP (VAMP) is designed to access an average contrast down to $\sim 10^{-6}$ in a full donut-shaped dark zone from 8 to 35λ/D. This enables to access objects from 167 to 546 mas within the full wavelength range. In the different filter bandwidths, VAMP accesses 135 to 546 mas (625 nm filter), 145 to 592 mas (675 nm filter), 157 to 637 mas (725 nm filter), 161 to 660 mas (750 nm filter), 167 to 683 mas (775 nm filter).

The final design is shown in Figure 4 (right), and Figure 5 (bottom) illustrates its coronagraphic PSFs in monochromatic light at 600 nm, 700 nm, and 800 nm, and in broadband light from 600 to 800 nm with an RGB combination of 41 wavelengths linearly spread between 600 and 800 nm. On the coronagraphic PSFs, the same two planets (off-axis sources) than in the CHAR1 and CHAR2 cases have been added to the simualtion.

3. APPLICATION SET UP AND POST-PROCESSING

3.1 Manufacturing

Both on CHARIS and on VAMPIRES, the RAP windows need to be circular with a 1 inch (25 mm) diameter and a thickness below 5 mm to fit in the wheels, with a surface parallelism below 5 arcsec, and each surface should have a flatness better than $\lambda/10$ or $\lambda/20$ at 633 nm. The CHARIS windows should be highly transmissive in the infrared, between 0.95 and 2.4 μm and will be set up in the apodizer wheel, where the pupil diameter is 17.92 mm. The VAMPIRES window has to be coated for visible light, more precisely 600 to 800 nm. Because there is no apodizer plane available, the RAP will be installed in the Lyot plane, where the pupil diameter is 7.03 mm. The apodizer windows are provided by Optimask, that also manufactured them as apodizers with photolithography with chromium metallization ($R < 10\%$), with a precision of 1 μm. Optimask also provided the anti-reflection coating required for SCExAO ($R < 1\%$, $0.95 - 2.4\mu$m for CHAR1 and CHAR2 and $600 - 800$nm for VAMP). Fig. 6 shows pictures of the three masks (left) and a zoom to CHAR1 (right) under a microscope.

3.2 Low-wind effect simulations

SCExAO is equiped with a Boston Micromachines DM, composed of 2000 actuators, meaning 45 actuators across the pupil diameter. With this DM, both static and dynamic LWE can be simumated with petal-level piston

and/or tip-tilt errors.[11,12] In our application case, we focus on static petal-level piston-like errors, from 0.001 to 3.1 rad rms of wavefront error, at $\lambda = 1550$ nm for CHAR1 and CHAR2 and $\lambda = 750$ nm for VAMP.

3.3 Image post-processing

Later on in this paper, all high-dynamic images have the same quick post-processing:

1) 500000 images with saturated intensity peak (exposure time T_S) are taken, with 500000 darks (same exposure time T_S). The darks are subtracted to the images, and the images are averaged to one single intensity image I_S.

2) 500000 images with non-saturated intensity peak (exposure time T_0) are taken, with 500000 darks (same exposure time T_0). The darks are subtracted to the images, and the images are averaged to one single image I_0.

3) The image I_S is normalized by $T_0/T_S \times 1/max(I_0)$.

4. RESULTS

The three apodizers have been manufactured by Optimask and sent to IPAG in July 2023. In September 2023, they were finally set up on SCExAO. The next few weeks have been dedicated to the RAP calibration and first results, with SCExAO internal source.

4.1 Performance and contrast curves

Fig. 7 (top) shows the three coronagraphic PSFs behind CHAR1, CHAR2, and VAMP after the processing described in section 3.3. The laser source is centered on 1550nm (25nm bandwidth) for CHAR1 and CHAR2, and on 750nm (50nm bandwidth) for VAMP. No aberration has been simulated here, and only the system aberrations limit the performance. Fig. 7 (bottom) indicates the contrast curves of the three coronagraphic PSFs, by computing their azimuthal average plots (in the case of CHAR2, only one quarter of the PSF is used).

Both CHAR1 and CHAR2 reach a contrast of $\sim 10^{-4}$ in their dark holes, meaning respectively a circular dark region from 8 to $37\lambda/D$ and a "prohibition" sign dark zone from 6 to $27\lambda/D$. VAMP generates a dark region from 9 to $37\lambda/D$, with a contrast at $\sim 3 \times 10^{-5}$. One can also notice that the overall performance is better with VAMP in terms of contrast than with CHAR1 and CHAR2, meaning a deeper contrast in the visible light than in the infrared light. We cannot explain this difference so far, since the instrument is supposed to be less impacted by aberrations at longer wavelengths.

4.2 Robustness to low-wind effect

We add controlled low-wind effect with petal-level piston errors on the DM and study the robustness of the three RAPs to such aberrations: in Fig. 8, one see the coronagraphic normalized PSFs behind the three masks for low-wind effect-like aberrations from 0.001 to 1 rad RMS, with no to little visual evolution of the PSFs.

In Fig. 9, we compute such PSFs for a larger number of aberration amplitudes and compute, for each case, the normalized PSF and the average contrast in its dark region. We obtain a "hockey-cross" like plot as already presented in the literature.[28–32] As expected for RAPs, optimized for coronagraphic PSF stability, the average contrast in the dark region remains stable up to a few radians, which corresponds to the loss of coherence of the PSF peak: the petals are then so unphased that each of them acts like a single imager, and the PSF peak energy is spread through the lobes generated by each petal.

5. CONCLUSIONS

This proceeding introduces the first experimental validation of the RAP concept, with three designs developed, installed, and tested for the SCExAO instrument at the Subaru telescope: CHAR1 and CHAR2 for the infrared CHARIS instrument, and VAMP for the visible light VAMPIRES instrument. For all three RAPs, the optimal performance is overall limited by the instrument internal aberrations, with contrasts down to $\sim 10^{-4}$ for both infrared RAPs and $\sim 3\times10^{-5}$ for VAMP. The robustness to LWE is as expected, meaning the dark zone contrast is maintained up to a couple radians, ie., the loss of coherence of the PSF core.

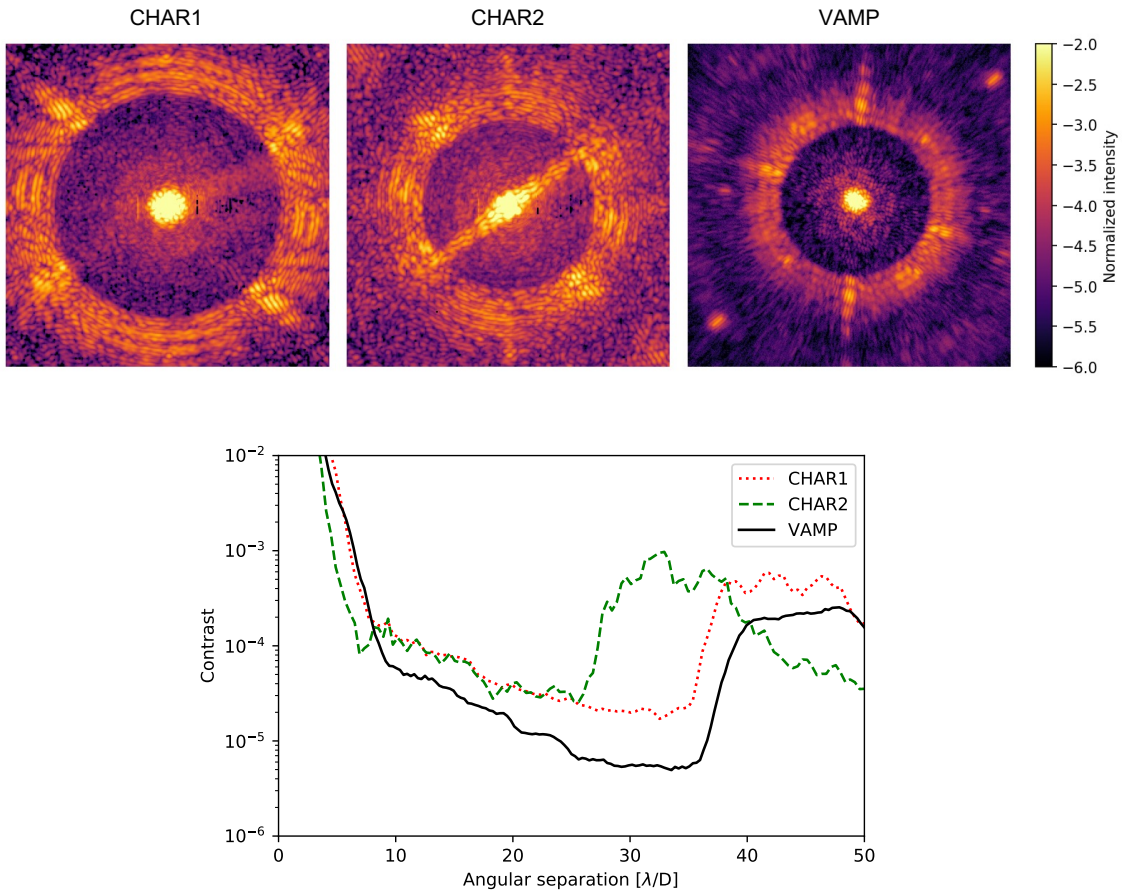

Figure 7. Performance after calibration: (top) calibrated images in internal source (1550 ± 12.5nm for CHAR1 and CHAR2, 750 ± 25nm for VAMP) without added aberration, (bottom) contrast curves of the three images above.

The next step is to test these three RAPs on sky with Subaru/SCExAO, which should be done in the coming year, and evaluate their performance and robustness in real conditions, including observation LWE.

Another application of the RAP concept would be the development of a RAP robust to primary mirror segmentation-induced aberrations, at higher contrast and closer IWA. The RAP concept would be of particular interest for an UV high-contrast instrument, since aberrations have a higher impact on the performance.

ACKNOWLEDGMENTS

This project benefited from fundings from the L'Oréal-UNESCO For Women in Science foundation and from CNRS that L.L. thanks for their financial support.

REFERENCES

[1] Beuzit, J. L., Vigan, A., Mouillet, D., Dohlen, K., Gratton, R., Boccaletti, A., Sauvage, J. F., Schmid, H. M., Langlois, M., Petit, C., Baruffolo, A., Feldt, M., Milli, J., Wahhaj, Z., Abe, L., Anselmi, U., Antichi, J., Barette, R., Baudrand, J., Baudoz, P., Bazzon, A., Bernardi, P., Blanchard, P., Brast, R., Bruno, P., Buey, T., Carbillet, M., Carle, M., Cascone, E., Chapron, F., Charton, J., Chauvin, G., Claudi, R., Costille, A., De Caprio, V., de Boer, J., Delboulbé, A., Desidera, S., Dominik, C., Downing, M., Dupuis, O., Fabron, C., Fantinel, D., Farisato, G., Feautrier, P., Fedrigo, E., Fusco, T., Gigan, P., Ginski, C., Girard, J., Giro, E., Gisler, D., Gluck, L., Gry, C., Henning, T., Hubin, N., Hugot, E., Incorvaia, S., Jaquet, M., Kasper, M.,

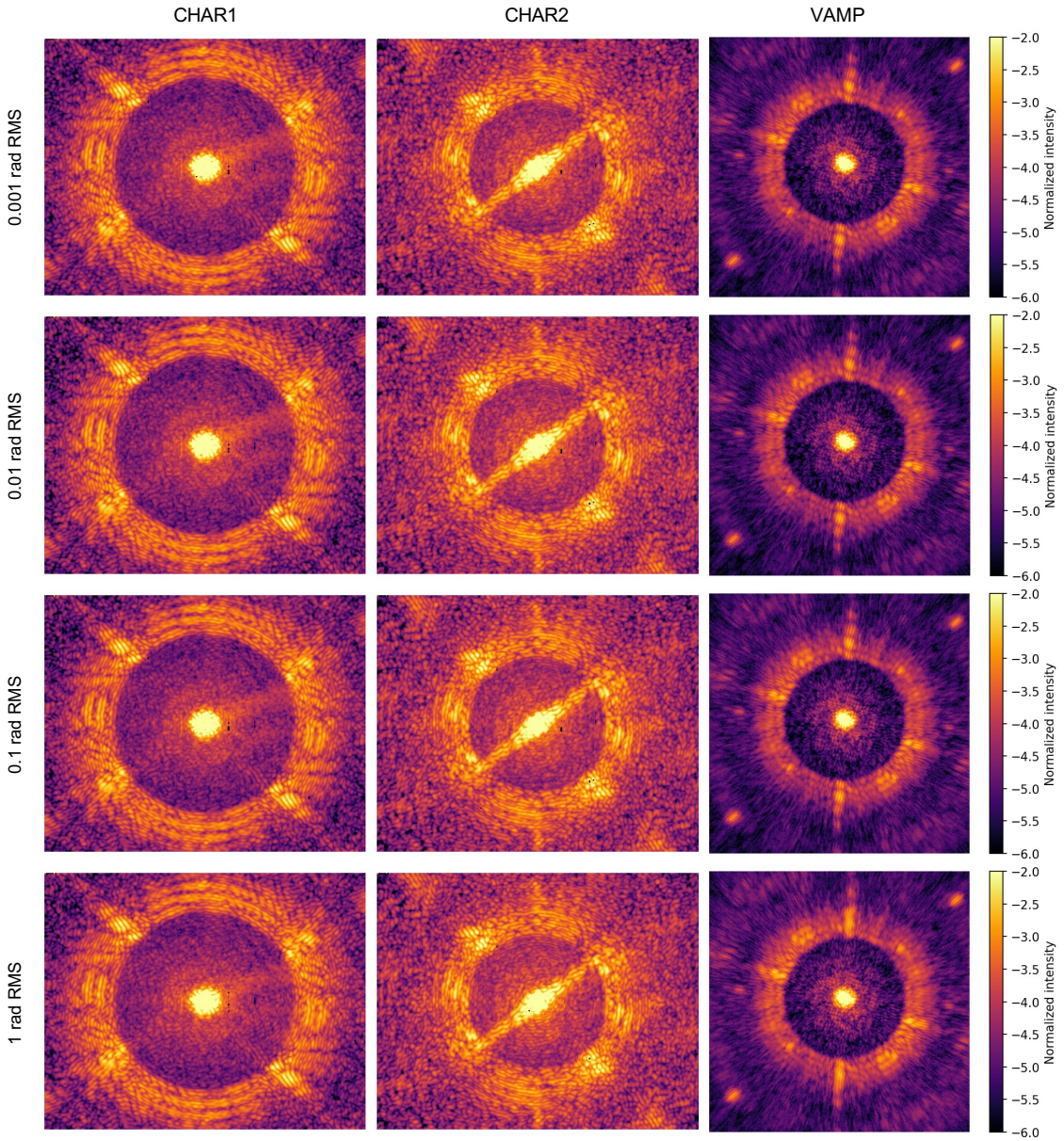

Figure 8. Coronagraphic PSF (normalized intensity in log scale) robustness to low-wind effect for (left) CHAR1, (center) CHAR2, and (right) VAMP, with increasing petal-level piston errors from (top) 0.001 rad RMS to (bottom) 1 rad RMS.

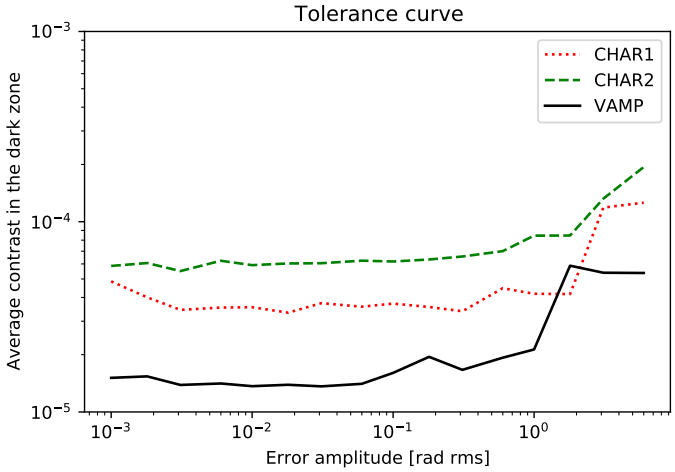

Figure 9. Impact of increasing petal-level piston errors on the average contrast of the dark regions generated by CHAR1, CHAR2, and VAMP.

Lagadec, E., Lagrange, A. M., Le Coroller, H., Le Mignant, D., Le Ruyet, B., Lessio, G., Lizon, J. L., Llored, M., Lundin, L., Madec, F., Magnard, Y., Marteaud, M., Martinez, P., Maurel, D., Ménard, F., Mesa, D., Möller-Nilsson, O., Moulin, T., Moutou, C., Origné, A., Parisot, J., Pavlov, A., Perret, D., Pragt, J., Puget, P., Rabou, P., Ramos, J., Reess, J. M., Rigal, F., Rochat, S., Roelfsema, R., Rousset, G., Roux, A., Saisse, M., Salasnich, B., Santambrogio, E., Scuderi, S., Segransan, D., Sevin, A., Siebenmorgen, R., Soenke, C., Stadler, E., Suarez, M., Tiphène, D., Turatto, M., Udry, S., Vakili, F., Waters, L. B. F. M., Weber, L., Wildi, F., Zins, G., and Zurlo, A., "SPHERE: the exoplanet imager for the Very Large Telescope," **631**, A155 (Nov. 2019).

[2] Sauvage, J.-F., Fusco, T., Guesalaga, A., Wizinowitch, P., O'Neal, J., N'Diaye, M., Vigan, A., Girard, J., Lesur, G., Mouillet, D., Buezit, J.-L., Kasper, M., Le Louarn, M., Mlli, J., Dohlen, K., Neichel, B., Bourget, P., Heigenauer, P., and Mawet, D., "Low Wind Effect, the main limitation of the SPHERE instrument," in [*Adaptive Optics for Extremely Large Telescopes IV (AO4ELT4)*], E9 (Oct. 2015).

[3] Sauvage, J.-F., Fusco, T., Lamb, M., Girard, J., Brinkmann, M., Guesalaga, A., Wizinowich, P., O'Neal, J., N'Diaye, M., Vigan, A., Mouillet, D., Beuzit, J.-L., Kasper, M., Le Louarn, M., Milli, J., Dohlen, K., Neichel, B., Bourget, P., Haguenauer, P., and Mawet, D., "Tackling down the low wind effect on SPHERE instrument," in [*Adaptive Optics Systems V*], Marchetti, E., Close, L. M., and Véran, J.-P., eds., *Society of Photo-Optical Instrumentation Engineers (SPIE) Conference Series* **9909**, 990916 (July 2016).

[4] Lamb, M. P., Correia, C., Sauvage, J.-F., Véran, J.-P., Andersen, D. R., Vigan, A., Wizinowich, P. L., van Dam, M. A., Mugnier, L., and Bond, C., "Quantifying telescope phase discontinuities external to adaptive optics systems by use of phase diversity and focal plane sharpening," *Journal of Astronomical Telescopes, Instruments, and Systems* **3**, 039001 (July 2017).

[5] Milli, J., Mouillet, D., Fusco, T., Girard, J. H., Masciadri, E., Pena, E., Sauvage, J. F., Reyes, C., Dohlen, K., Beuzit, J. L., Kasper, M., Sarazin, M., and Cantalloube, F., "Performance of the extreme-AO instrument VLT/SPHERE and dependence on the atmospheric conditions," *arXiv e-prints* , arXiv:1710.05417 (Oct. 2017).

[6] Milli, J., Kasper, M., Bourget, P., Pannetier, C., Mouillet, D., Sauvage, J. F., Reyes, C., Fusco, T., Cantalloube, F., Tristam, K., Wahhaj, Z., Beuzit, J. L., Girard, J. H., Mawet, D., Telle, A., Vigan, A., and N'Diaye, M., "Low wind effect on VLT/SPHERE: impact, mitigation strategy, and results," in [*Adaptive Optics Systems VI*], Close, L. M., Schreiber, L., and Schmidt, D., eds., *Society of Photo-Optical Instrumentation Engineers (SPIE) Conference Series* **10703**, 107032A (July 2018).

[7] Cantalloube, F., Dohlen, K., Milli, J., Brandner, W., and Vigan, A., "Peering through SPHERE Images: A Glance at Contrast Limitations," *The Messenger* **176**, 25–31 (June 2019).

[8] Holzlöhner, R., Kimeswenger, S., Kausch, W., and Noll, S., "Bolometric night sky temperature and subcooling of telescope structures," **645**, A32 (Jan. 2021).

[9] Pourré, N., Le Bouquin, J. B., Milli, J., Sauvage, J. F., Fusco, T., Correia, C., and Oberti, S., "Low-wind-effect impact on Shack-Hartmann-based adaptive optics. Partial control solution in the context of SPHERE and GRAVITY+," **665**, A158 (Sept. 2022).

[10] N'Diaye, M., Martinache, F., Jovanovic, N., Lozi, J., Guyon, O., Norris, B., Ceau, A., and Mary, D., "Calibration of the island effect: Experimental validation of closed-loop focal plane wavefront control on Subaru/SCExAO," **610**, A18 (Feb. 2018).

[11] Vievard, S., Bos, S., Cassaing, F., Ceau, A., Guyon, O., Jovanovic, N., Keller, C. U., Lozi, J., Martinache, F., Montmerle-Bonnefois, A., Mugnier, L., NDiaye, M., Norris, B., Sahoo, A., Sauvage, J.-F., Snik, F., Wilby, M. J., and Wong, A., "Overview of focal plane wavefront sensors to correct for the Low Wind Effect on SUBARU/SCExAO," *arXiv e-prints* , arXiv:1912.10179 (Dec. 2019).

[12] Vievard, S., Bos, S. P., Cassaing, F., Currie, T., Deo, V., Guyon, O., Jovanovic, N., Keller, C. U., Lamb, M., Lopez, C., Lozi, J., Martinache, F., Miller, K., Montmerle-Bonnefois, A., Mugnier, L. M., N'Diaye, M., Norris, B., Sahoo, A., Sauvage, J. F., Skaf, N., Snik, F., Wilby, M. J., and Wong, A., "Focal plane wavefront sensing on SUBARU/SCExAO," in [*Adaptive Optics Systems VII*], Schreiber, L., Schmidt, D., and Vernet, E., eds., *Society of Photo-Optical Instrumentation Engineers (SPIE) Conference Series* **11448**, 114486D (Dec. 2020).

[13] Bos, S. P., Vievard, S., Wilby, M. J., Snik, F., Lozi, J., Guyon, O., Norris, B. R. M., Jovanovic, N., Martinache, F., Sauvage, J. F., and Keller, C. U., "On-sky verification of Fast and Furious focal-plane wavefront sensing: Moving forward toward controlling the island effect at Subaru/SCExAO," **639**, A52 (July 2020).

[14] Wilby, M. J., Keller, C. U., Sauvage, J. F., Fusco, T., Mouillet, D., Beuzit, J. L., and Dohlen, K., "A "Fast and Furious"' solution to the low-wind effect for SPHERE at the VLT," in [*Adaptive Optics Systems V*], Marchetti, E., Close, L. M., and Véran, J.-P., eds., *Society of Photo-Optical Instrumentation Engineers (SPIE) Conference Series* **9909**, 99096C (July 2016).

[15] Leboulleux, L., Carlotti, A., and N'Diaye, M., "Redundant apodization for direct imaging of exoplanets. I. Robustness to primary mirror segmentation-induced errors outside the segment diffraction limit," **659**, A143 (Mar. 2022).

[16] Leboulleux, L., Carlotti, A., N'Diaye, M., Bertrou-Cantou, A., Milli, J., Pourré, N., Cantalloube, F., Mouillet, D., and Vérinaud, C., "Redundant apodization for direct imaging of exoplanets. II. Application to island effects," **666**, A91 (Oct. 2022).

[17] Peters-Limbach, M. A., Groff, T., Kasdin, N. J., McElwain, M. W., Galvin, M., Carr, M. A., Lupton, R., Gunn, J. E., Knapp, G., Gong, Q., Carlotti, A., Brandt, T., Janson, M., Guyon, O., Martinache, F., Hayashi, M., and Takato, N., "Conceptual design of the Coronagraphic High Angular Resolution Imaging Spectrograph (CHARIS) for the Subaru telescope," in [*Ground-based and Airborne Instrumentation for Astronomy IV*], McLean, I. S., Ramsay, S. K., and Takami, H., eds., *Society of Photo-Optical Instrumentation Engineers (SPIE) Conference Series* **8446**, 84467U (Sept. 2012).

[18] Peters-Limbach, M. A., Groff, T. D., Kasdin, N. J., Driscoll, D., Galvin, M., Foster, A., Carr, M. A., LeClerc, D., Fagan, R., McElwain, M. W., Knapp, G., Brandt, T., Janson, M., Guyon, O., Jovanovic, N., Martinache, F., Hayashi, M., and Takato, N., "The optical design of CHARIS: an exoplanet IFS for the Subaru telescope," in [*Techniques and Instrumentation for Detection of Exoplanets VI*], Shaklan, S., ed., *Society of Photo-Optical Instrumentation Engineers (SPIE) Conference Series* **8864**, 88641N (Sept. 2013).

[19] Groff, T. D., Kasdin, N. J., Limbach, M. A., Galvin, M., Carr, M. A., Knapp, G., Brandt, T., Loomis, C., Jarosik, N., Mede, K., McElwain, M. W., Leviton, D. B., Miller, K. H., Quijada, M. A., Guyon, O., Jovanovic, N., Takato, N., and Hayashi, M., "The CHARIS IFS for high contrast imaging at Subaru," in [*Techniques and Instrumentation for Detection of Exoplanets VII*], Shaklan, S., ed., *Society of Photo-Optical Instrumentation Engineers (SPIE) Conference Series* **9605**, 96051C (Sept. 2015).

[20] Groff, T., Chilcote, J., Brandt, T., Kasdin, N. J., Galvin, M., Loomis, C., Rizzo, M., Knapp, G., Guyon, O., Jovanovic, N., Lozi, J., Currie, T., Takato, N., and Hayashi, M., "First light of the CHARIS high-contrast integral-field spectrograph," in [*Society of Photo-Optical Instrumentation Engineers (SPIE) Conference*

Series], Shaklan, S., ed., *Society of Photo-Optical Instrumentation Engineers (SPIE) Conference Series* **10400**, 1040016 (Sept. 2017).

[21] 't Hart, J. G. J., van Holstein, R. G., Bos, S. P., Ruigrok, J., Snik, F., Lozi, J., Guyon, O., Kudo, T., Zhang, J., Jovanovic, N., Norris, B., Martinod, M.-A., Groff, T. D., Chilcote, J., Currie, T., Tamura, M., Vievard, S., Sahoo, A., Deo, V., Ahn, K., Martinache, F., and Kasdin, J., "Full characterization of the instrumental polarization effects of the spectropolarimetric mode of SCExAO/CHARIS," in [*Polarization Science and Remote Sensing X*], Kupinski, M. K., Shaw, J. A., and Snik, F., eds., *Society of Photo-Optical Instrumentation Engineers (SPIE) Conference Series* **11833**, 118330O (Aug. 2021).

[22] Wang, J. J., Gao, P., Chilcote, J., Lozi, J., Guyon, O., Marois, C., De Rosa, R. J., Sahoo, A., Groff, T. D., Vievard, S., Jovanovic, N., Greenbaum, A. Z., and Macintosh, B., "Atmospheric Monitoring and Precise Spectroscopy of the HR 8799 Planets with SCExAO/CHARIS," **164**, 143 (Oct. 2022).

[23] Ruane, G., Riggs, A., Mazoyer, J., Por, E. H., N'Diaye, M., Huby, E., Baudoz, P., Galicher, R., Douglas, E., Knight, J., Carlomagno, B., Fogarty, K., Pueyo, L., Zimmerman, N., Absil, O., Beaulieu, M., Cady, E., Carlotti, A., Doelman, D., Guyon, O., Haffert, S., Jewell, J., Jovanovic, N., Keller, C., Kenworthy, M. A., Kuhn, J., Miller, K., Sirbu, D., Snik, F., Wallace, J. K., Wilby, M., and Ygouf, M., "Review of high-contrast imaging systems for current and future ground- and space-based telescopes I: coronagraph design methods and optical performance metrics," in [*Space Telescopes and Instrumentation 2018: Optical, Infrared, and Millimeter Wave*], Lystrup, M., MacEwen, H. A., Fazio, G. G., Batalha, N., Siegler, N., and Tong, E. C., eds., *Society of Photo-Optical Instrumentation Engineers (SPIE) Conference Series* **10698**, 106982S (Aug. 2018).

[24] Uyama, T., Norris, B., Jovanovic, N., Lozi, J., Tuthill, P., Guyon, O., Kudo, T., Hashimoto, J., Tamura, M., and Martinache, F., "High-contrast Hα imaging with Subaru/SCExAO + VAMPIRES," *Journal of Astronomical Telescopes, Instruments, and Systems* **6**, 045004 (Oct. 2020).

[25] Lucas, M., Bottom, M., Guyon, O., Lozi, J., Norris, B., Deo, V., Vievard, S., Ahn, K., Skaf, N., and Tuthill, P., "A visible-light Lyot coronagraph for SCExAO/VAMPIRES," in [*Ground-based and Airborne Instrumentation for Astronomy IX*], Evans, C. J., Bryant, J. J., and Motohara, K., eds., *Society of Photo-Optical Instrumentation Engineers (SPIE) Conference Series* **12184**, 121844E (Aug. 2022).

[26] Norris, B., Schworer, G., Tuthill, P., Jovanovic, N., Guyon, O., Stewart, P., and Martinache, F., "The VAMPIRES instrument: imaging the innermost regions of protoplanetary discs with polarimetric interferometry," **447**, 2894–2906 (Mar. 2015).

[27] Lucas, M., Norris, B., Guyon, O., Bottom, M., Deo, V., Vievard, S., Lozi, J., Ahn, K., Ashcraft, J., Currie, T., Doelman, D., Kudo, T., Leboulleux, L., Lilley, L., Millar-Blanchaer, M., Safonov, B., Tuthill, P., Uyama, T., Walk, A., and Zhang, M., "The Next Generation of Visible High-Contrast Imaging and Polarimetry with SCExAO/VAMPIRES,"

[28] Stahl, M. T., Shaklan, S. B., and Stahl, H. P., "Preliminary analysis of effect of random segment errors on coronagraph performance," in [*Techniques and Instrumentation for Detection of Exoplanets VII*], Shaklan, S., ed., *Society of Photo-Optical Instrumentation Engineers (SPIE) Conference Series* **9605**, 96050P (Sept. 2015).

[29] Stahl, H. P., "Advanced Mirror Technology Development (AMTD) project: overview and year four accomplishments," in [*Advances in Optical and Mechanical Technologies for Telescopes and Instrumentation II*], Navarro, R. and Burge, J. H., eds., *Society of Photo-Optical Instrumentation Engineers (SPIE) Conference Series* **9912**, 99120S (July 2016).

[30] Leboulleux, L., Sauvage, J.-F., Pueyo, L. A., Fusco, T., Soummer, R., Mazoyer, J., Sivaramakrishnan, A., N'Diaye, M., and Fauvarque, O., "Pair-based Analytical model for Segmented Telescopes Imaging from Space for sensitivity analysis," *Journal of Astronomical Telescopes, Instruments, and Systems* **4**, 035002 (July 2018).

[31] Laginja, I., Soummer, R., Mugnier, L. M., Pueyo, L., Sauvage, J.-F., Leboulleux, L., Coyle, L., and Knight, J. S., "Analytical tolerancing of segmented telescope co-phasing for exo-Earth high-contrast imaging," *Journal of Astronomical Telescopes, Instruments, and Systems* **7**, 015004 (Jan. 2021).

[32] Laginja, I., Sauvage, J.-F., Mugnier, L. M., Pueyo, L., Perrin, M. D., Noss, J., Will, S. D., Brooks, K. J., Por, E. H., Petrone, P., and Soummer, R., "Wavefront tolerances of space-based segmented telescopes at very high contrast: Experimental validation," **658**, A84 (Feb. 2022).